Pharmaceutical Research, Vol. 26, No. 8, August 2009 (© 2009)
DOI: 10.1007/s11095-009-9915-1

Research Paper

Drug Delivery to the Skin From Sub-micron Polymeric Particle Formulations: Influence of Particle Size and Polymer Hydrophobicity

Xiao Wu,[1,2] Bruno Biatry,[3] Colette Cazeneuve,[4] and Richard H. Guy[1,5]

Received April 27, 2009; accepted May 20, 2009; published online June 10, 2009

Purpose. To investigate the influence of particle size and polymer properties on the topical delivery of a lipophilic "active" species (Nile Red (NR)) from sub-micron polymeric particles.
Methods. Three poly-(ε-caprolactone) (CAPA) formulations were examined to assess the impact of particle size. Three other formulations, based on cellulose acetate butyrate (CAB), CAPA and polystyrene were studied to address the role of polymer hydrophobicity. *In vitro* skin permeation, and confocal microscopy and stratum corneum (SC) tape-stripping were used to evaluate the cutaneous disposition of NR.
Results. NR delivery into the SC was greater from the larger particles, the overall smaller surface area of which enhanced the "leaving tendency" of the lipophilic "active". Skin uptake of NR (measured as "% payload released") from polystyrene, CAPA and CAB particles increased with decreasing polymer hydrophobicity (polystyrene>CAPA>CAB) as expected. Confocal microscopy revealed that NR released from the particles accumulated in, and penetrated via, lipid domains between the SC corneocytes. The particles showed affinity for hairs, and concentrated on the skin surface at the follicular openings.
Conclusions. Delivery of a model drug to the skin from sub-micron polymeric particle formulations is sensitive to the particle size and the relative hydrophobicity of the carrier.

KEY WORDS: laser scanning confocal microscopy (LSCM); skin; sub-micron particles; tape-stripping.

INTRODUCTION

The development of nanotechnology, and the increasing presence of sub-micron particles (and other structures of similar dimensions) in pharmaceutical and cosmetic formulations designed for application to the skin (1–7), makes it essential to develop techniques to assess the local disposition of these materials. Although the principal function of the skin is to provide a protective barrier (a job that it performs remarkably well) (8–10), it is nevertheless important to determine whether sub-micron structures can find their way into and/or across this tissue, or whether they show a particular affinity, for example, to specific skin components such as hairs and the follicles from which hairs emerge.

A number of fundamental questions must therefore be addressed. For example, what happens to sub-micron particles when they contact the skin? What is the disposition of the particles, and what is their residence time? It is necessary, therefore, to visualize particle disposition on and within the skin, to explore whether penetration pathways exist, and to examine the "substantivity" of the sub-micron structures to the membrane. Further, is there evidence that such particles can cross the skin's barrier, the stratum corneum (SC)? Do the particles show affinity for specific skin structures, e.g., hair follicles? Microscopic techniques and adhesive tape-stripping procedures can be used to address these issues qualitatively and quantitatively. Finally, to what extent does particle disposition depend on the properties of the particles (such as size and composition)? What happens to "active" species (e.g., drugs, cosmetic actives) which are associated with sub-micron particles?

This paper addresses these latter issues, and explores the manner in which particle size and polymer hydrophobicity influence the cutaneous disposition of a model, lipophilic compound associated with various "vectors". Uptake into the skin's outermost layer, the SC, has been determined by a validated and quantitative adhesive tape-stripping methodology and has been visualized by confocal microscopy.

[1] Department of Pharmacy & Pharmacology, University of Bath, Claverton Down, Bath, BA2 7AY, UK.
[2] College of Pharmacy, University of Kentucky, Lexington, Kentucky 40536-0082, USA.
[3] L'Oréal Research, F-94550, Chevilly-Larue, France.
[4] L'Oréal Research, F-93601, Aulnay-sous-Bois, France.
[5] To whom correspondence should be addressed. (e-mail: r.h.guy@bath.ac.uk)

ABBREVIATIONS: CAB, cellulose acetate butyrate; CAPA, poly-(ε-caprolactone); LSCM, laser scanning confocal microscopy; NR, Nile Red; PI, polydispersity index; PS, polystyrene; SC, stratum corneum; TEWL, transepidermal water loss.

MATERIALS AND METHODS

Chemicals

Poly-(ε-caprolactone) (CAPA 6100, MW 10000, Solvay, UK), cellulose acetate butyrate (CAB-551-0.01, MW16000, Eastman, Capelle aan den IJssel, the Netherlands), polystyrene (ref. 18544, MW 50000, PolySciences, Eppelheim, Germany), Phenonip (Nipa, Clariant, Charlotte, NC, USA), dimethicone copolyol (SH 3773M, Dow Corning Toray, Japan), disodium stearoyl glutamate (Amisoft HS21P, Ajinomoto, Japan), Nile Red (Analytical grade, Sigma-Aldrich, St. Louis, MO, USA), dichloromethane (99% Acros Organics, Loughborough, UK), acetonitrile (HPLC grade, Fisher Scientific Corporation, Loughborough, UK).

Skin Tissue

Full thickness porcine skin was obtained from a local slaughterhouse. The skin was cleaned under cold running water and the subcutaneous fat was removed with a scalpel. The remaining tissue was then dermatomed to a thickness of ~750 μm and was stored frozen at −20°C for up to a maximum of one month before use.

Sub-Micron Particle Preparation

Particles were prepared in the presence of the model "active", Nile Red (NR), a lipophilic fluorophore, by a mini-emulsion/solvent evaporation method adapted from (11). 1.25 g polymer, 0.25 g dimethicone copolyol and 1.25 mg Nile Red were dissolved in 17 ml dichloromethane, to form the organic phase. 0.125 g Amisoft HS21P was dissolved in 25 ml water by vigorously stirring the mixture at 40°C for 30 minutes to provide the aqueous phase. The organic phase was introduced into the aqueous phase under high mixing (Ultra turrax® T25, tool 25F, 12000 rpm) at 4°C for 5 min. The pre-emulsion was then sonicated (Branson Sonifier 450, power=10, 30% cycle, large probe) at 4°C during 10 min. Finally, the organic solvent (dichloromethane) and some of the water present were removed by rotary evaporation under vacuum at 40°C. Phenonip was added into the emulsion as a preservative.

Size Distribution Measurement

The mean size and polydispersity index of the particles were measured with dynamic light scattering (BI90Plus, Brookhaven Instruments Corporation, NY, USA). The polydispersity index reflects the size distribution of the dispersion and, for example, a value of 0.1 indicates a very narrow size distribution (monodisperse). Measurements were made in triplicate for all prepared batches.

Assessment of Nile Red Incorporation and HPLC Assay

To determine the degree of Nile Red incorporation into the particles, the formulations were filtered (0.45 μm nylon filters, Whatman, Japan) and then subjected to ultracentrifugation at 17000 g for 3 h at 20°C. The supernatant was kept for analysis of NR. The sediment was washed with distilled water to remove surfactant and again centrifuged 17000 g for 3 h. The resulting pellet was freeze-dried, and then dissolved in dichloromethane. Finally, Nile Red in this organic solvent was measured by HPLC (Dionex, Sunnyvale, CA, USA) with fluorescence detection at 559 nm and 630 nm for excitation and emission wavelengths, respectively. A Hypersil BDS C18 (5 μm) 250×4.6 mm column, was used and the mobile phase was dichloromethane pumped at a flow rate of 1 ml/min at 25°C. Each injection was 200 μl of solution. The Nile Red retention time was 5.6 min. Nile Red in the supernatant was also measured by HPLC using a mobile phase comprising acetonitrile-water (80:20). The column, injection volume, temperature were as above. The retention time in this case was 12.1 min.

In vitro Skin Permeation

Each skin sample used in these experiments represented one-half of a larger piece of tissue. The other portion was reserved for a determination of the SC thickness as described below.

Visible hairs on the skin were trimmed as closely as possible to the surface. Skin permeation experiments were performed in vertical Franz diffusion cells thermostatted at 37°C. The excised tissue was clamped between the donor and receptor compartments exposing a diffusion area of 3.8 cm^2. The receptor phase was physiological buffer (pH=7.4); the donor compartment held 1 ml of the polymeric particle formulation and was covered with Parafilm. After an application lasting 6 h, the cell was dismantled, and the skin was immediately either examined by confocal microscopy or tape-stripped to determine the NR concentration profile across the SC.

SC Tape-Stripping

A validated tape-stripping procedure was used to assess the depth of NR penetration into the SC and recover NR from the treated skin. About 20 pieces of 2.7×2.7 cm square tapes were prepared using transparent Scotch® No.845 Book Tapes (3M Media, Broken, Germany). To delimit a fixed area for tape stripping, a 5×5 cm square mask was prepared with a cut central aperture of 2 cm in diameter. A strip of adhesive tape was pressed firmly onto the skin surface, and then removed in a single movement. The direction of stripping was changed with each tape to ensure a more uniform removal of the SC with fewer tape-strips. Before and after each tape-strip, transepidermal water loss (TEWL) across the skin was measured with an Aquaflux device (Biox Systems Ltd., London, UK) to provide an idea of when most of the SC had been removed and to terminate the tape-stripping process. This was considered appropriate when TEWL reached 80 $g^{-1}m^{-2}h$. The tapes were weighed before and after stripping to determine the mass of SC removed. As the density of the tissue is ~1 g/cm^3 (12,13), the volume of SC removed by each strip is known assuming uniform coverage of SC on the tape-strip (12). Then, given that the area stripped is kept at a known, constant value, the thickness of SC removed as tape-stripping proceeds can be found.

NR was extracted from the SC on the adhesive tapes by immersion in acetonitrile and shaking for at least 12 h. The

Table I. Properties of Sub-micron Polymeric Particle Formulations Examined

Particle formulation			% Nile Red associated	% Nile Red in supernatant
(polymer)	Average diameter (nm)	PI[a]	(mean±SD)	(mean±SD)
CAPA	90	0.172	46.3±1.1	5.8±0.2
CAPA	260	0.108	48.0±1.6	5.8±0.4
CAPA	630	0.116	48.6±0.8	5.8±0.3
PS	156	0.098	76.9±2.0	5.8±0.4
CAPA	148	0.133	48.6±0.5	5.8±0.3
CAB	93	0.125	23.9±1.5	5.8±0.4

[a] PI: polydispersity index of the size distribution (expressed using a 0–1 scale)

extract was filtered (Whatman PTFE filter 0.45 µm) into HPLC vials and analysed. The mobile phase was 80:20 v/v acetonitrile and water. All other HPLC conditions were as stated above. The limits of detection and quantification were 0.34 ng/ml and 1.16 ng/ml, respectively.

SC Thickness Determination

To calculate the total thickness of the SC, the same tape-stripping procedure was performed on the second skin sample with measurements of TEWL after each tape-strip (12). The amount of SC removed on each tape was again determined gravimetrically and converted into a SC thickness removed on each strip. It was then possible to calculate the total thickness of the SC from the x-intercept of a graph of $TEWL^{-1}$ *versus* the cumulative thickness of SC removed (x) (12). Knowing the SC thickness of each skin used in the NR uptake experiments made it possible to express all concentration profiles of the "active" as a common function of the relative position (depth) into the SC, greatly facilitating objective comparison of the results (14,15).

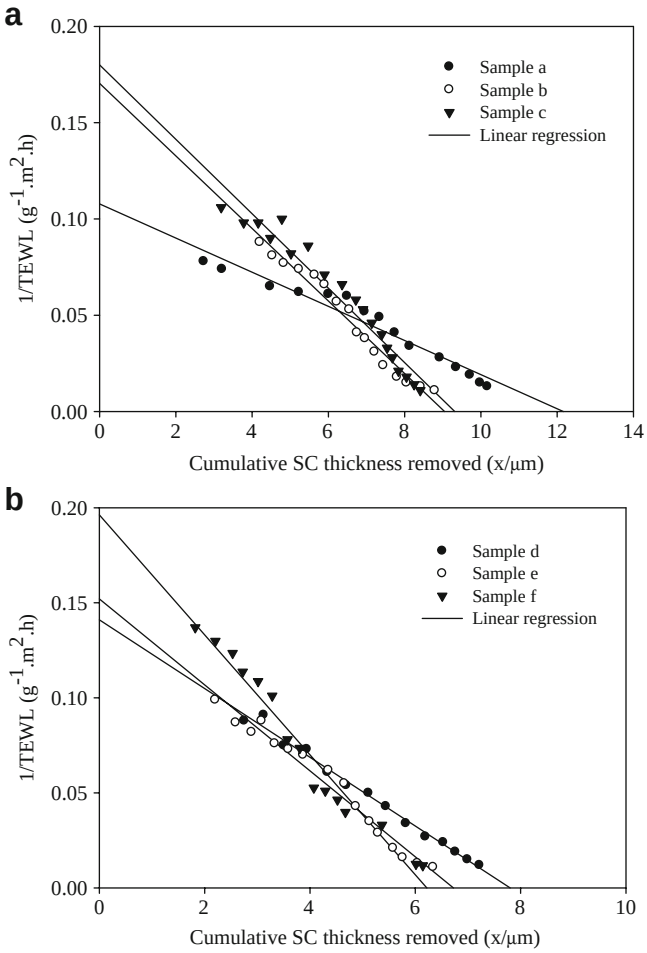

Fig. 1. Illustrative experimental data for the determination of SC thickness (obtained from the x-axis intercepts of the above plots). Results in panel (**a**) were from dorsal skin samples, those in panel (**b**) from the abdomen.

Laser Scanning Confocal Microscopy (LSCM)

The treated skin was cleaned carefully with physiological buffer and dried with tissue. The skin was examined using a LSM 510 Invert Laser Scanning Microscope (Carl Zeiss, Jena, Germany). The system was equipped with a HeNe laser (excitation line at 543 nm). A Plan-Neofluar 10×/0.3 objective, EC Plan-Neofluar 40 ×/1.30 oil DIC M27 objective and Plan-Apochromat 63 ×/1.40 oil DIC M27 objective were used. Confocal images were obtained in the plane parallel to the sample surface (xy-mode), or in the plane perpendicular (optical sectioning z-stack mode).

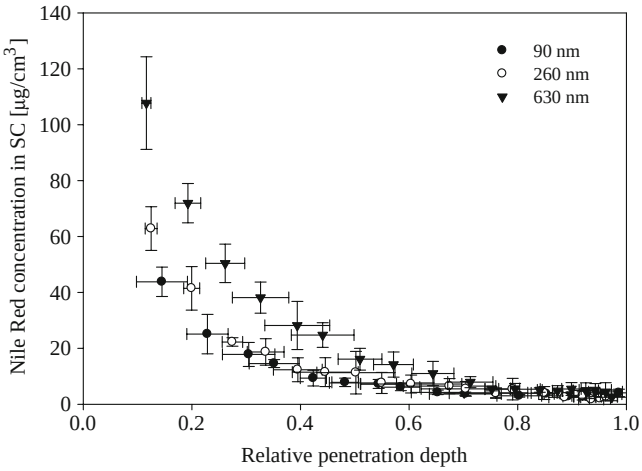

Fig. 2. SC concentration profiles of NR following a 6-hour application of CAPA particles having mean diameters of 90 nm, 260 nm and 630 nm (n=5; mean±SD). Note that, on the x-axis, 0 indicates the SC surface, 1 reflects the SC-stratum granulosum interface.

Table II. Values of K, D/L^2 and Accumulated Amount of NR in the SC (mean±SD, n=5) After 6-hour Application of Three Sub-micron Particle Formulations with Different Particle Size

Particle diameter (nm)	K^a	D/L^2 (h^{-1}) [b]	Total quantity of NR recovered from tape-strips (μg)
90	2170±103	0.007±0.002	0.023
260	3026±555	0.007±0.003	0.033
630	4669±810	0.008±0.002	0.058

[a] Partition coefficient estimated by fitting the permeation data to Eq. 1

[b] Diffusion coefficient divided by the diffusion length squared estimated by fitting the permeation data to Eq. 1

RESULTS AND DISCUSSION

Nile Red Association with Sub-Micron Polymeric Particles

The quantities of NR incorporated into the particles, together with information on their size and polydispersity are summarized in Table I. Uptake into the particles made from CAPA was quite constant (46–49%). More NR was taken up into the hydrophobic PS particles (~77%), less into the more hydrophilic CAB formulation (~24%). A relatively constant amount of Nile Red was recovered in the supernatant for all particles, and it is inferred that the remaining fraction of the dye was associated with surfactant micelles.

SC Thickness Determination

Fig. 1 shows typical results from the experiments conducted to determine SC thickness of the skin samples used in the NR uptake measurements. The variability between different skins is clear, and it was generally observed that SC on the abdomen of the pig was thinner than that on the dorsal surface (6.9±0.8 μm *versus* 10.2±1.7 μm, respectively, for the examples in Fig. 1, mean±SD, n=3). These results emphasize the value of the determination of SC thickness when the disposition of an "active" across the barrier is to be evaluated, as it means that all concentrations can be expressed on a common scale of SC penetration depth normalized by the total membrane thickness (see below).

NR Concentration Profiles Across the SC

In all experiments, independent of the formulation used, no fluorescence from NR was ever detected in the receptor phase, an observation consistent with earlier work (16,17).

The SC concentration profiles of Nile Red delivered from CAPA particles of different average diameters are in Fig. 2. From the measurements of TEWL and of the SC mass removed on each tape, the concentrations could be expressed

Fig. 3. Illustration of the contact area between particles and the surface of stratum corneum; a larger particle has a bigger contact area than a smaller one.

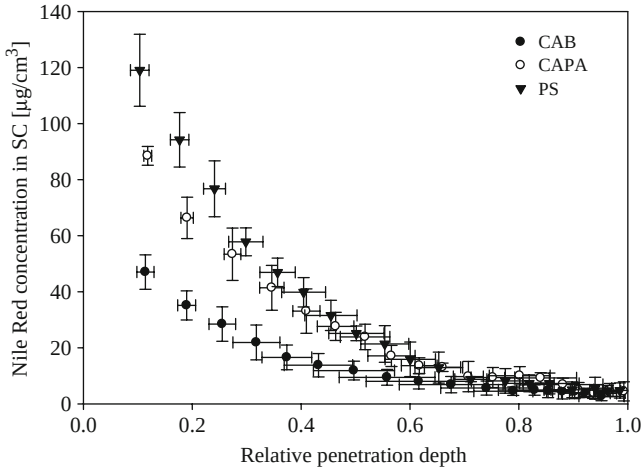

Fig. 4. SC concentration profiles of NR following a 6-hour application of PS, CAPA and CAB particles (n=5; mean±SD).

as a function of relative position within the SC (as reported before (15)), thereby correcting for differences in absolute SC thickness from one porcine skin sample to another. The effectiveness of this strategy is reflected in the excellent reproducibility in the results obtained.

As the NR concentration (C_{veh}) in each formulation was known, the SC concentration (C_x) *versus* normalized depth (x/L) profiles of NR in Fig. 2 were fitted to the appropriate solution of Fick's second law of diffusion (Eq. 1).

$$C_x = K \cdot C_{veh}\left\{1 - \frac{x}{L} - \frac{2}{\pi}\sum_{n=1}^{\infty}\frac{1}{n}\cdot\sin(n\pi x/L)\cdot\exp\left(-Dn^2\pi^2 t/L^2\right)\right\} \quad (1)$$

This equation assumes that (i) the applied NR concentration remains constant for the treatment period (t); (ii) the viable epidermis is a perfect sink for the permeant; (iii) the SC contains no NR at t=0. The fitting procedure yielded the SC/vehicle partition coefficient (K) of NR and its characteristic diffusion parameter (D/L^2, where D is NR's diffusivity across the SC of thickness L). In addition, the accumulated amount of NR in the SC at the end of the application period was determined by summing the quantities recovered from the individual tape-strips. The quantitative results are collected in Table II.

The data imply that NR is more efficiently transferred into the SC from the polymeric vectors as the particle size increases. As the precise localization of NR in the CAPA

Table III. Values of K, D/L^2 and Accumulated Amount of NR in the SC (mean±SD, n=5) After 6-hour Application of Three Sub-micron Particle Formulations Made From Different Polymers

Particles (polymer)	K^a	D/L^2 (h^{-1})[b]	Total quantity of NR recovered from tape-strips (μg)
PS	3393±267	0.011±0.002	0.053
CAPA	3839±126	0.014±0.002	0.038
CAB	4182±631	0.014±0.005	0.029

[a] Partition coefficient estimated by fitting the permeation data to Equation 1

[b] Diffusion coefficient divided by the diffusion length squared estimated by fitting the permeation data to Equation 1.

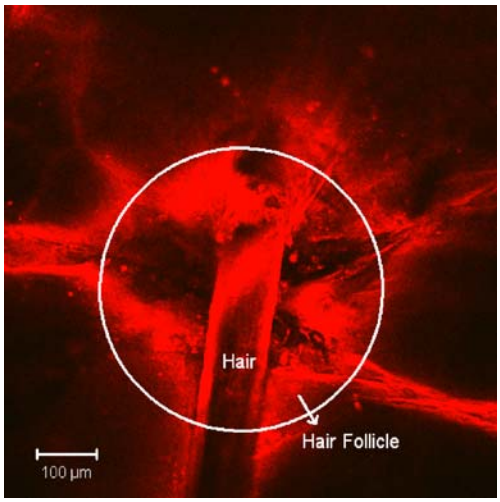

Fig. 5. Confocal image (×10) of the skin surface following a 6-hour application of CAPA particles (90 nm diameter) containing NR. Clear localization around a hair follicle is observed.

particles is not known, an unambiguous explanation for the observations is not possible. However, if, as suspected, NR is predominantly absorbed onto the particle surface, then the larger carriers obviously offer a smaller surface area and the "leaving tendency" of NR from the vehicle would be enhanced. This would be reflected, of course, in a larger value of the partition coefficient and a greater quantity of NR recovered, both of which were seen. Furthermore, the larger particles have bigger contact areas with the surface of SC than the smaller particles, which could also facilitate the partitioning of NR into the SC (Fig. 3).

Fig. 4 shows the concentration profiles of NR in porcine SC following delivery of the active from PS, CAPA and CAB particles. The partition coefficient (K), diffusivity parameter (D/L^2) of NR transport across the skin, and total quantity of NR recovered from individual tape-strips are shown in Table III. Uptake of the lipophilic "active" was greatest (0.053 µg) from the most hydrophobic polymer (PS) and least (0.029 µg) from the most hydrophilic (CAB), with that from CAPA (of intermediate properties) falling in between (0.038 µg). These differences are influenced, of course, by the different loadings of NR achieved into the different particles (Table I): the "payloads" for PS, CAPA and CAB were 77%, 49% and 24%, respectively. If the SC uptake levels are normalized by these different fractional loadings (i.e., average amounts of the dye taken up into the SC are divided by the fraction of the active eventually associated with the particles), the resulting ratios are 0.69 for PS, 0.78 for CAPA and 1.20 for CAB indicating, as would be expected, that NR release from the least hydrophobic particle (into the lipophilic SC) is favored relative to that from the more hydrophobic polymer, which is also reflected in the partition coefficient (K).

Visualization of NR Disposition in the SC by Confocal Microscopy

To visualize fluorescently-labeled biological samples, laser scanning confocal microscopy (LSCM) is a very valuable tool. Its optical sectioning function provides in-depth information of thick specimens without perturbation or destruction of the sample (18). Confocal images from the surface of skin treated with sub-micron polymeric particles revealed the disposition of the associated NR post-application. Fig. 5, for example, shows intense red fluorescence around a clearly imaged hair follicle following application of the CAPA 90 nm diameter particles. The affinity of polymeric particles for such appendageal structures has been reported previously (17). Fig. 6 illustrates NR distribution at the surface of the stratum corneum and nicely outlines the polygonal shapes of the corneocytes (19,20). Not surprisingly, therefore, the NR released from (in this case, CAB) particles enters the SC via the intercellular lipid domains.

Fig. 7 illustrates the use of LSCM to optically section through the skin to produce a z-stack series of images as a function of depth into the SC and upper epidermis. In this example, NR released from CAB particles is seen to penetrate via the intercellular pathway but that it is effectively constrained to the SC, with little evidence of deeper

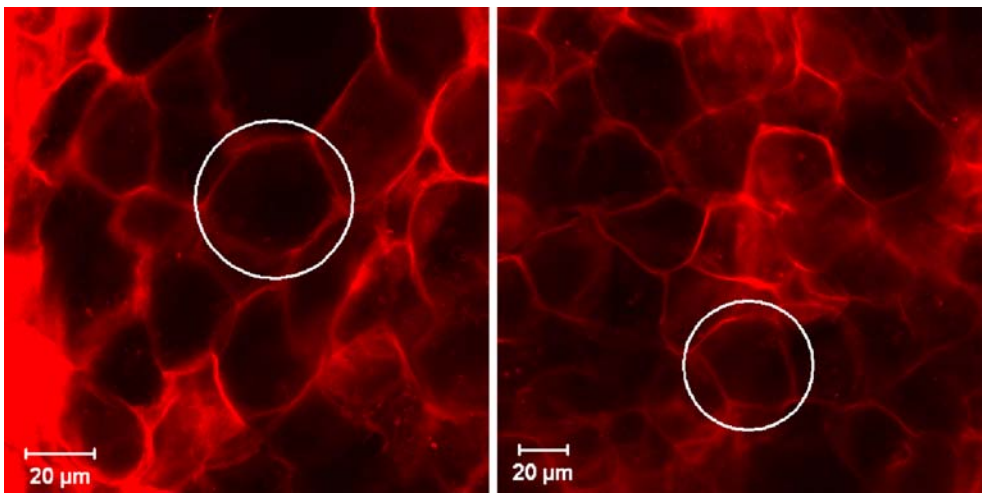

Fig. 6. Confocal image (×63) of the skin surface following a 6-hour application of CAB particles containing NR. The release of the fluorophore into the intercellular lipid domains clearly outlines the polygonal shapes of the SC corneocytes.

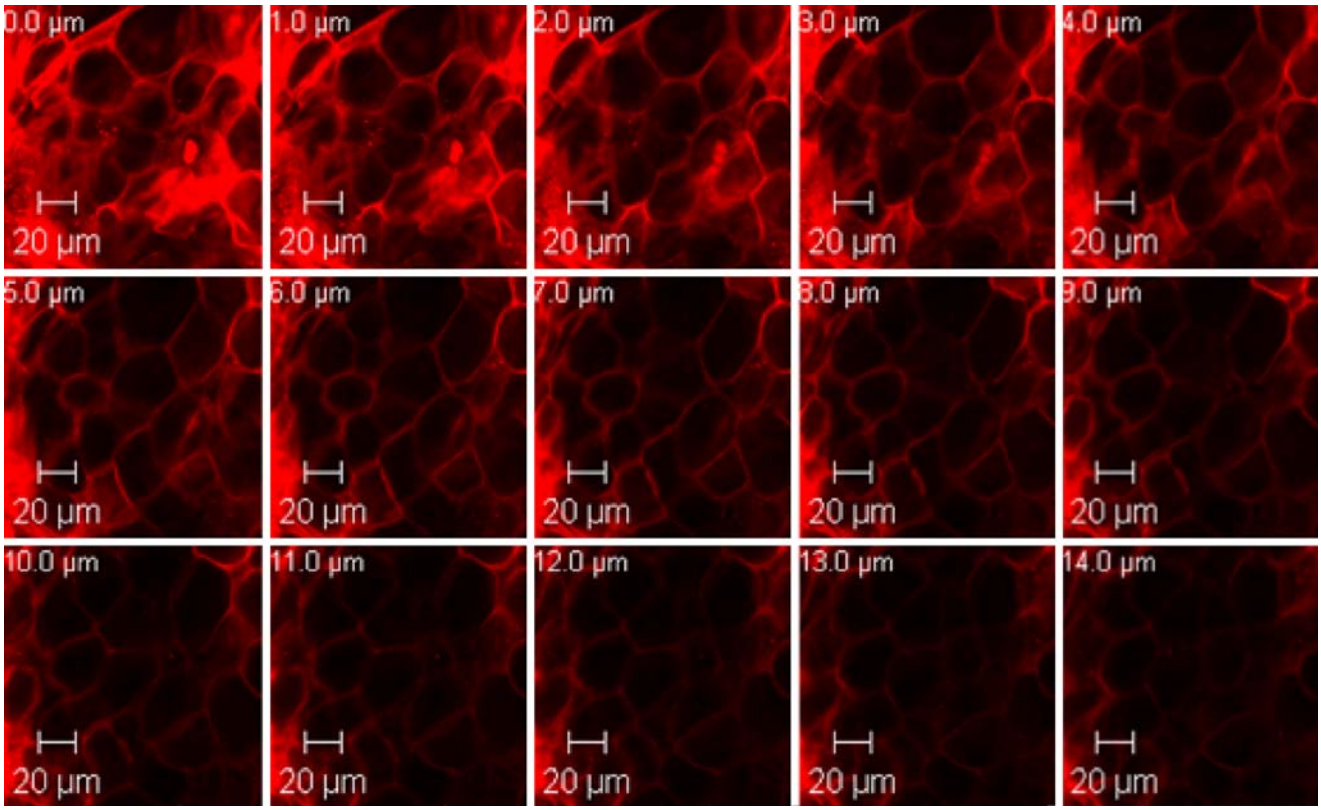

Fig. 7. Optical sectioning images (×63) of skin after a 6-hour application of CAB particles containing NR. The sample area was imaged as the focus plane of the LSCM was lowered in steps of 1 µm.

transport during the 6-hour application period. Fig. 8 demonstrates how the z-stack images can be "reconstructed" to provide a cross-sectional image of the skin by sectioning through a specified plane. The NR released from the CAPA 90 nm diameter particles is limited in its disposition to the upper layer (primarily the SC) of the skin. Only in the vicinity of a hair follicle is there evidence for deeper penetration of the fluorescence.

Additionally, skin samples may be mechanically sectioned in the normal way and then examined by LSCM at a plane beyond the cut surface (thereby avoiding artifacts associated with the sectioning procedure). This provides an alternative approach to obtain information about penetration into the deeper skin layers and has the advantage that it overcomes the progressive loss of resolution and signal with depth within the tissue, due to scattering and absorption of both the laser excitation and fluorescence emission light (21,22). An example of this approach is illustrated in Fig. 9, which captures a hair follicle exiting the skin and demonstrates once more that NR uptake is limited to the SC.

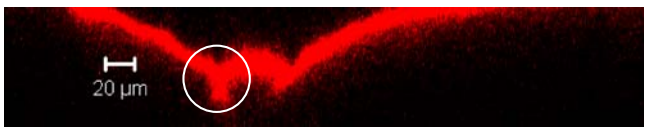

Fig. 8. Reconstructed, optical cross-sectional image (×10) of skin after a 6-hour application of CAPA (90 nm diameter) particles containing NR. Penetration of the fluorophore is mostly constrained to the SC to a depth of ~10 µm, but is occasionally visualized further into the tissue around hair follicles as highlighted by the white circle.

CONCLUSIONS

The size and the hydrophobicity of sub-micron polymeric particles clearly influence the local disposition of an associated, lipophilic "active" species when applied to the skin. Larger particles, with a relatively smaller total surface area encourage the "active" to enter the lipophilic stratum corneum more

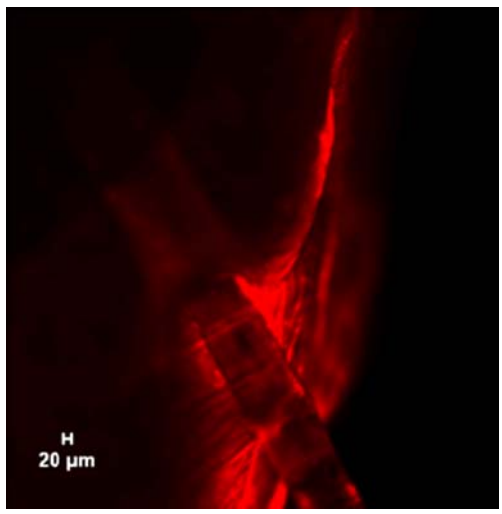

Fig. 9. LSCM image of a mechanical cross-section of skin following a 6-hour application of CAB particles containing NR. The fluorophore was visualized in the SC and around a hair follicle but did not penetrate into deeper regions of skin.

efficiently. Particles made with more hydrophobic polymers are able to bring a greater "payload" of the lipophilic active to the skin surface and the absolute uptake into the SC is higher than that from less hydrophobic carriers. However, when delivery is more appropriately viewed as the fraction of the payload transferred from particle to skin, the expected, improved release from the least hydrophobic polymer (i.e., that least sympathetic to the lipophilic "active") is observed.

Confocal microscopy reveals that the released "active" diffuses into the SC via the intercellular lipids but that it is constrained exclusively to this, the skin's outermost, barrier layer. Affinity of the formulations for appendageal structures, such as hair follicles, is clear, but the present study is unable to distinguish whether the red fluorescence seen is free "active", or "active" still associated with the particles. Resolution of this key question forms the basis of future work.

ACKNOWLEDGEMENTS

Supported by the European Commission 6th Research and Technological Development Framework Programme (NAPOLEON: NAnostructured waterborne POLymEr films with OutstaNding properties) and a University Research Scholarship for Xiao Wu.

REFERENCES

1. Magdassi S. Delivery systems in cosmetics. Colloids Surf, A: Physicochem Eng Aspects. 1997;123-124:671–9. doi:10.1016/S0927-7757(97)03792-8.
2. Luppi B, Cerchiara T, Bigucci F, Basile R, Zecchi V. Polymeric nanoparticles composed of fatty acids and polyvinylalcohol for topical application of sunscreens. J Pharm Pharmacol. 2004;56:407–11. doi:10.1211/0022357022926.
3. Kaur IP, Agrawal R. Nanotechnology: a new paradigm in cosmeceuticals. Recent Pat Drug Deliv Formul. 2007;1:171–82. doi:10.2174/187221107780831888.
4. Shefer A, Shefer S. Controlled delivery system for hair care products. U.S. patent 6,491,902.
5. Soane DS, Linford MR. Nanoscopic hair care products. U.S. patent 6,821,509.
6. Quellet C, Hotz J, Balmer M. Polymeric nanoparticles including olfactive components. U.S. patent 7,205,340.
7. Alvarez-Roman R, Barre G, Guy RH, Fessi H. Biodegradable polymer nanocapsules containing a sunscreen agent: preparation and photoprotection. Eur J Pharm Biopharm. 2001;52:191–5. doi:10.1016/S0939-6411(01)00188-6.
8. Wertz PW, Downing DT. Stratum corneum: biological and biochemical considerations. In: Hadgraft J, Guy RH, editors. Transdermal drug delivery. New York: Marcel Dekker, Inc; 1989. p. 1–22.
9. Downing DT, Stewart ME, Wertz PW, Colton SW, Abraham W, Strauss JS. Skin lipids: an update. J Invest Dermatol. 1987;88:2s–6s. doi:10.1111/1523-1747.ep12468850.
10. Potts RO, Guy RH. Predicting skin permeability. Pharm Res. 1992;9:663–9. doi:10.1023/A:1015810312465.
11. Chernysheva YV, Babak VG, Kildeeva NR, Boury F, Benoit JP, Ubrich N, *et al.* Effect of the type of hydrophobic polymers on the size of nanoparticles obtained by emulsification - solvent evaporation. Mendeleev Commun. 2003;13:65–7. doi:10.1070/MC2003v013n02ABEH001690.
12. Kalia YN, Pirot F, Guy RH. Homogeneous transport in a heterogeneous membrane: water diffusion across human stratum corneum *in vivo*. Biophys J. 1996;71:2692–700. doi:10.1016/S0006-3495(96)79460-2.
13. Anderson RL, Cassidy JM. Variation in physical dimensions and chemical composition of human stratum corneum. J Invest Dermatol. 1973;61:30–2. doi:10.1111/1523-1747.ep12674117.
14. Kalia YN, Alberti I, Sekkat N, Curdy C, Naik A, Guy RH. Normalization of stratum corneum barrier function and trans-epidermal water loss *in vivo*. Pharm Res. 2000;17:1148–50. doi:10.1023/A:1026474200575.
15. Kalia YN, Alberti I, Naik A, Guy RH. Assessment of topical bioavailability *in vivo*: the importance of stratum corneum thickness. Skin Pharmacol Appl Skin Physiol. 2001;14(Suppl 1):82–6. doi:10.1159/000056394.
16. Jenning V, Gysler A, Schafer-Korting M, Gohla SH. Vitamin A loaded solid lipid nanoparticles for topical use: occlusive properties and drug targeting to the upper skin. Eur J Pharm Biopharm. 2000;49:211–8. doi:10.1016/S0939-6411(99)00075-2.
17. Alvarez-Roman R, Naik A, Kalia YN, Guy RH, Fessi H. Skin penetration and distribution of polymeric nanoparticles. J Control Release. 2004;99:53–62. doi:10.1016/j.jconrel.2004.06.015.
18. Shotton DM. Confocal scanning optical microscopy and its application for biological specimens. J Cell Sci. 1989;94:175–206.
19. Christophers E. Cellular architecture of the stratum corneum. J Invest Dermatol. 1971;56:165–9. doi:10.1111/1523-1747.ep12260765.
20. Mackenzie JC. Ordered structure of the stratum corneum of mammalian skin. Nature. 1969;222:881–2. doi:10.1038/222881a0.
21. Hoogstraate AJ, Cullander C, Nagelkerke JF, Spies F, Verhoef J, Schrijvers AHGJ, *et al.* A novel *in-situ* model for continuous observation of transient drug concentration gradients across buccal epithelium at the microscopical level. J Control Release. 1996;39:71–8. doi:10.1016/0168-3659(95)00140-9.
22. Laurent M, Johannin G, Gillbert N, Lucas L, Cassio D, Petit PX, *et al.* Power and limits of laser scanning confocal microscopy. Biol Cell. 1994;80:229–40. doi:10.1016/0248-4900(94)90046-9.